

Supporting Information

Sky-blue Thermally Activated Delayed Fluorescence Material Employing Diphenylethyne Acceptor for Organic Light-Emitting Diode Application

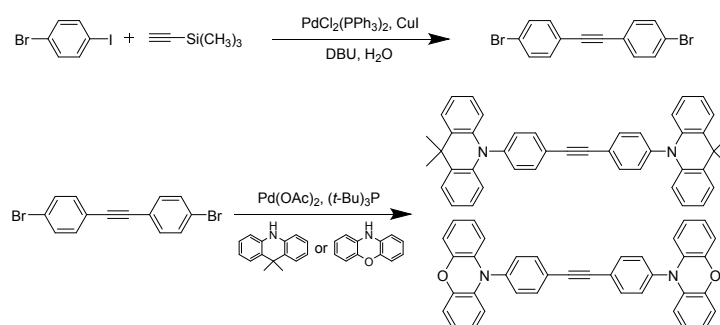
Zuozheng He,[†] Xinyi Cai,[†] Zhiheng Wang, Yunchuan Li, Zhida Xu, Kunkun Liu,
Dongcheng Chen, and Shi-Jian Su*

State Key Laboratory of Luminescent Materials and Devices and Institute of Polymer
Optoelectronic Materials and Devices, South China University of Technology,
Guangzhou 510640, China

[†]The authors contribute equally to this work.

*Corresponding author. E-mail: mssjsu@scut.edu.cn

Synthesis. All solvents and reagents were used as received from commercial suppliers without any further purification. Synthetic routes of the compounds are shown in **Scheme S1**, and they were further purified by repeated temperature gradient vacuum sublimation.



Scheme S1. Synthetic routes of the investigated compounds.

Synthesis of 1,2-bis(4-bromophenyl)ethyne (DPE-2Br):

A solution of 1-bromo-4-iodobenzene (3 g, 10 mmol) was dissolved in toluene (50 mL) in a three necked 100 mL flask. Bis(triphenylphosphine)palladium(II) chloride ($\text{PdCl}_2(\text{PPh}_3)_2$, 421 mg, 6 mol%), CuI (190 mg, 10 mol%), 1,8-diazabicyclo[5.4.0]undec-7-ene (DBU) (8.8 mL, 60 mmol) and (trimethylsilyl)acetylene (0.69 mL, 5 mmol) were added under N_2 atmosphere, followed by the addition of H_2O (72 μL , 0.4 eq.). The reaction mixture was stirred at room temperature in the dark overnight. Upon completion of the reaction, HCl was poured into the crude mixture and then it was extracted with chloroform. The organic layer was dried over anhydrous Na_2SO_4 , and the solvent removed under reduced pressure. The crude product was purified by silica gel column chromatography using petroleum ether (PE) as eluent, to give a yellow powder in 60% yield (2 g). ^1H NMR (500 MHz, chloroform-*d*) δ 7.51 – 7.46 (m, 4H), 7.40 – 7.35 (m, 4H).

Synthesis of 1,2-bis(4-(9,9-dimethylacridin-10(9H)-yl)phenyl)ethyne (DPE-DDMAc):

(1,2-Bis(4-bromophenyl)ethyne (1 g, 3 mmol), 9,9-dimethyl-9,10-dihydroacridine (1.4 g, 6.6 mmol), and K_2CO_3 (2.4 g, 18 mmol) were added into a 100 mL three neck flask with 60 mL toluene in N_2 atmosphere. After degassing for 15 min, acetic acid palladium (II) (67.2 mg, 0.3 mmol) and *tert*-butylphosphine (1 mL, 1 mmol) were added. Subsequently, the mixture was stirred and refluxed overnight, and then cooled to room temperature. After removing the solvent in vacuum, the mixture was partitioned between DCM and water. The combined organic layers were washed with brine, dried over Mg_2SO_4 and purified by column chromatography on silica gel (eluent: DCM/PE=3/1), affording a white solid in 80% yield (1.4 g). ^1H NMR (500 MHz, chloroform-*d*) δ 7.87 – 7.79 (m, 4H), 7.47 (dd, J = 7.6, 1.7 Hz, 4H), 7.40 – 7.33 (m, 4H), 7.04 – 6.89 (m, 8H), 6.31 (dd, J = 8.2, 1.3 Hz, 4H), 1.70 (s, 12H). ^{13}C NMR (126 MHz, chloroform-*d*) δ 141.44, 140.68, 140.66, 134.19, 131.77, 131.74, 131.56, 131.26, 131.19, 130.15, 126.45, 126.41, 125.30, 125.21, 125.14, 123.02, 120.82, 120.78, 120.69, 114.02, 113.89, 89.74, 36.00, 31.22, 31.02, 30.99. MALDI-TOF MS (mass m/z): calc 592.2878, found 592.2883 [M^+].

Synthesis of 1,2-bis(4-(10H-phenoxazin-10-yl)phenyl)ethyne (DPE-DPXZ):

(1,2-Bis(4-bromophenyl)ethyne (1 g, 3 mmol), 10H-phenoxazine (1.2 g, 6.6 mmol), and K_2CO_3 (2.4 g, 18 mmol) were added into a 100 mL three neck flask with 60 mL toluene in N_2 atmosphere. After

degassing for 15 min, acetic acid palladium (II) (67.2 mg, 0.3 mmol) and tri-*tert*-butylphosphine (1 mL, 1 mmol) were added. Subsequently, the mixture was stirred and refluxed overnight, and then cooled to room temperature. After removing the solvent in vacuum, the mixture was partitioned between DCM and water. The combined organic layers were washed with brine, dried over Mg₂SO₄ and purified by column chromatography on silica gel (eluent: DCM/PE=3/1), affording a white solid in 82% yield (1.3 g). ¹H NMR (500 MHz, chloroform-*d*) δ 7.83 – 7.73 (m, 4H), 7.42 – 7.33 (m, 4H), 6.82 – 6.46 (m, 12H), 6.02 – 5.90 (m, 4H). ¹³C NMR (126 MHz, chloroform-*d*) δ 143.96, 139.15, 134.34, 133.99, 131.10, 123.27, 123.22, 121.62, 115.55, 113.24, 89.69. MALDI-TOF MS (mass *m/z*): calc 540.1871, found 540.1843 [M⁺].

Chemical Characterization.

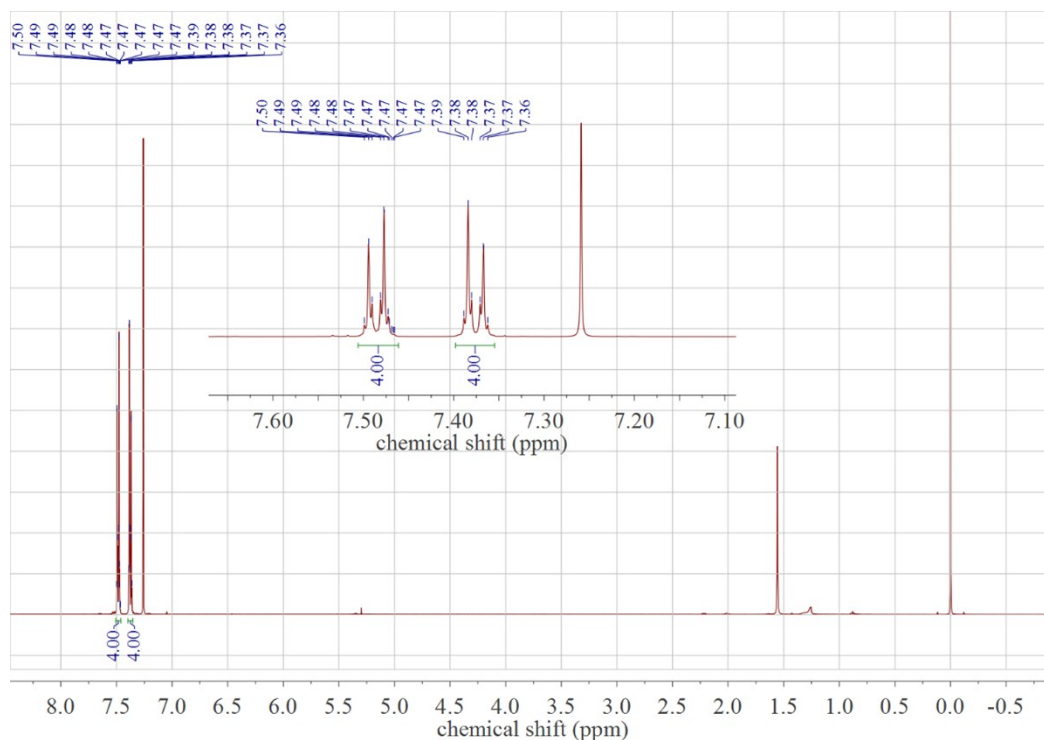


Fig. S1. ¹H NMR spectrum of compound DPE-2Br in deuterated CDCl₃.

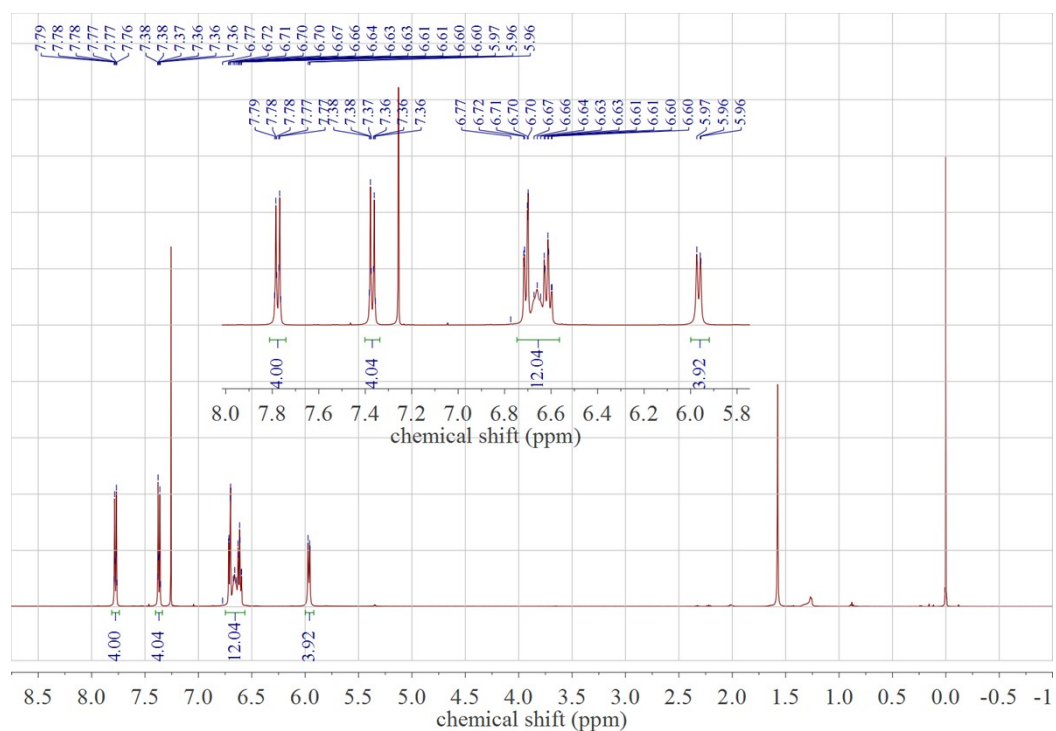


Fig. S4. ^1H NMR spectrum of compound DPE-DPXZ in deuterated CDCl_3 .

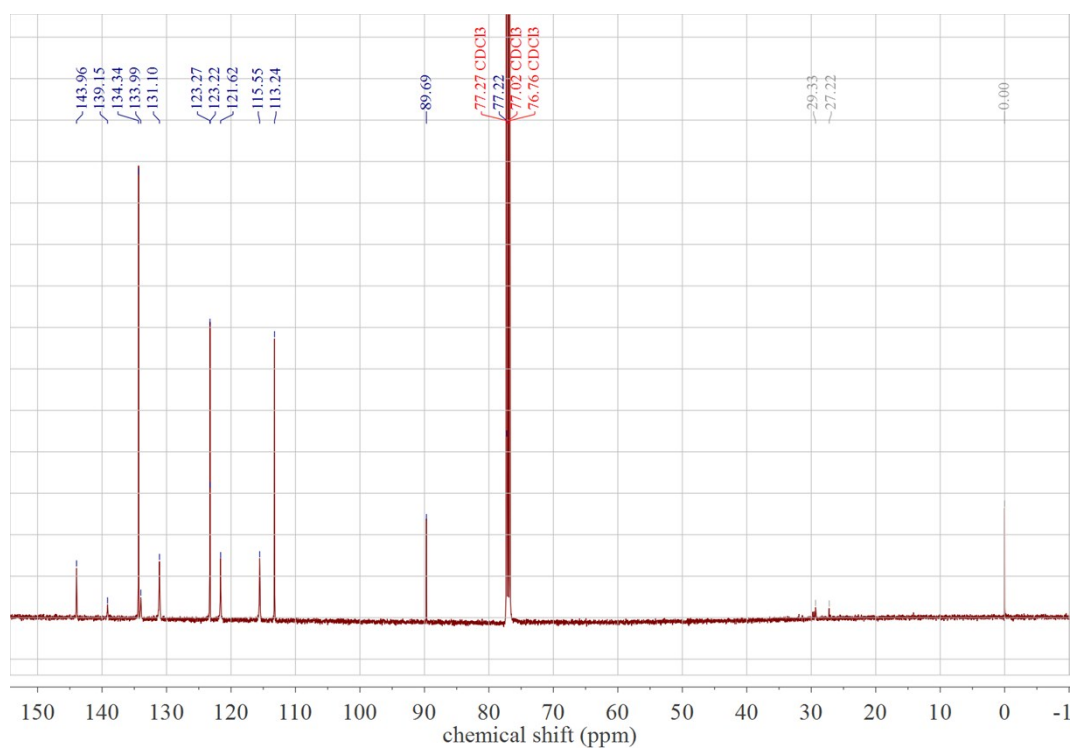


Fig. S5. ^{13}C NMR spectrum of compound DPE-DPXZ in deuterated CDCl_3 .

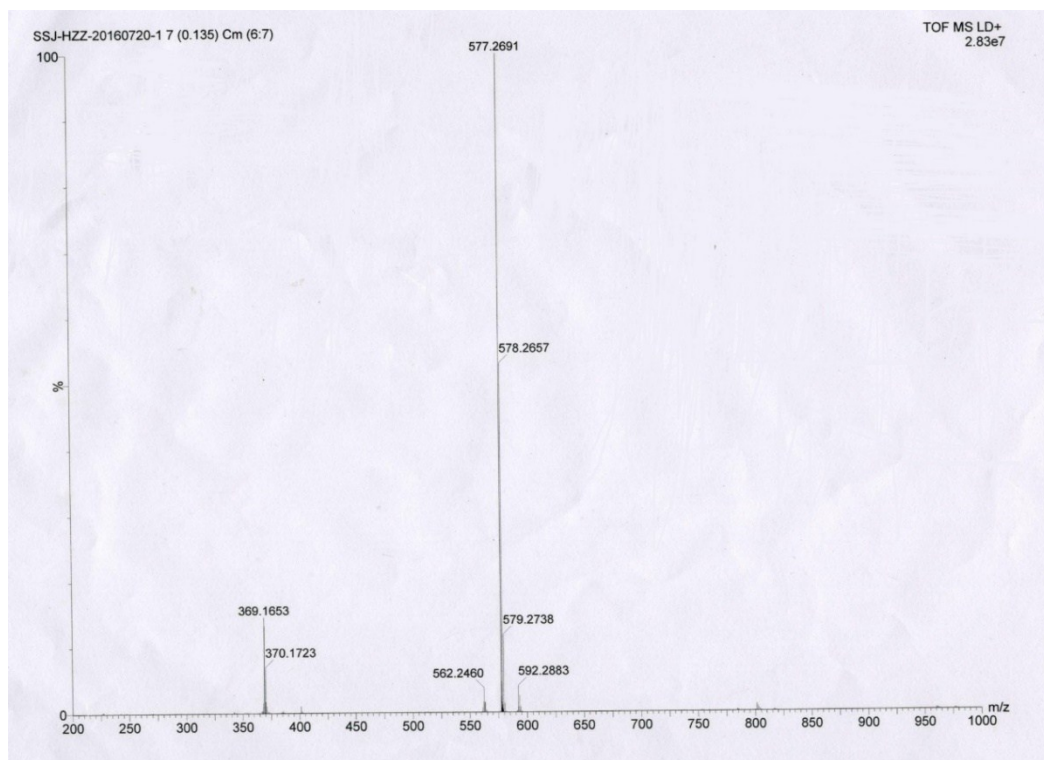


Fig. S6. MALDI-TOF mass spectrum of compound DPE-DDMAc.

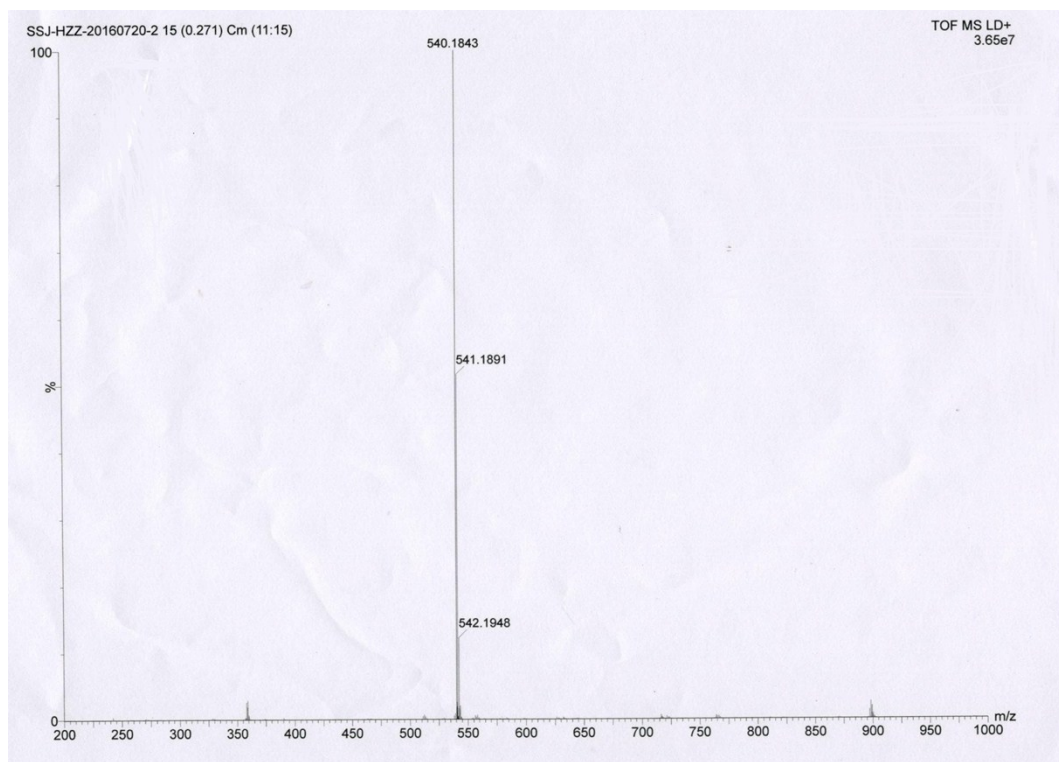


Fig. S7. MALDI-TOF mass spectrum of compound DPE-DPXZ.

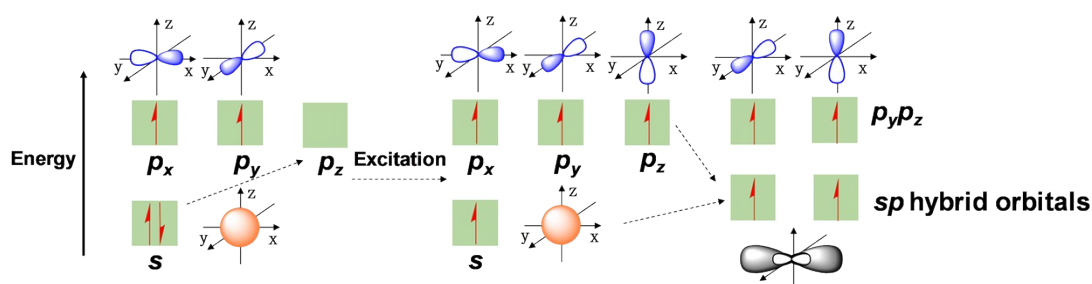


Fig. S8. Schematic diagram of sp hybrid orbitals.

Computation.

Computational details: All of the simulations were performed using the Gaussian 09_B01 program package.¹⁻³ Detailed calculation approach affording E_{0-0} (1CT), E_{0-0} (3CT) and E_{0-0} (3LE) are Equations S1 to S3.

$$E_{0-0}(^1CT) = E_{VA}(S_1, OHF) - 0.24 \quad (S1)$$

$$E_{0-0}(^3CT) = E_{0-0}(S_1) - \left[E_{VA}(S_1, OHF) - \frac{E_{VA}(S_1, OHF)}{E_{VA}(S_1, B3LYP)} E_{VA}(T_1, B3LYP) \right] \quad (S2)$$

$$E_{0-0}(^3LE) = E_{VA}(T_1) / [E_{VA}(S_1, OHF) / E_{VA}(S_1, B3LYP)] - 0.09 \quad (S3)$$

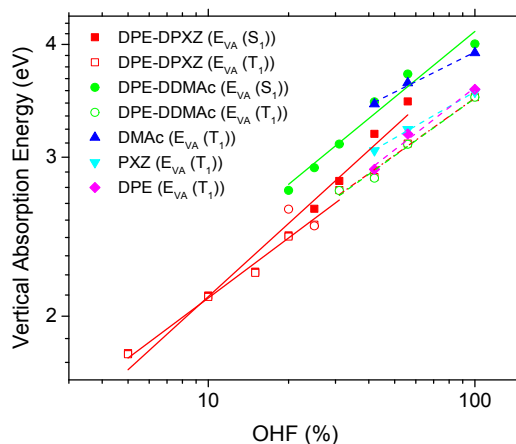


Fig. S9. Vertical absorption energy depending on HF% curves of the final compounds DPE-DPXZ and DPE-DDMAc as well as those of the intermediates (DMAc, PXZ and DPE) are shown for comparison.

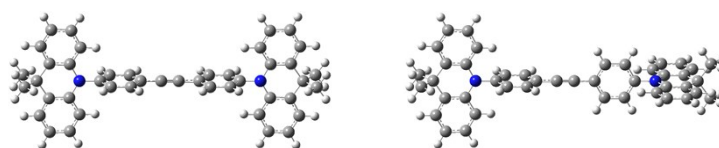


Fig. S10. Front views of horizontal oriented backbone (-1807.84419541 a.u.) and vertical oriented backbone (-1807.84288910 a.u.) DPE-DDMAc optimized in gas phase in B3LYP/6-31G* level. We tentatively took the horizontal oriented backbone one as the initial guess for the subsequent

simulation for its ground state energy is lower than the vertical oriented backbone one.

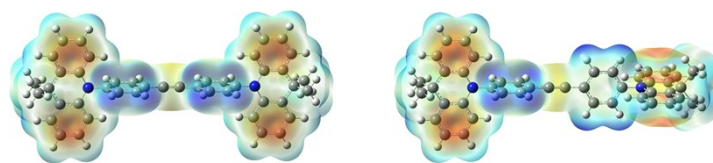


Fig. S11. Electrostatic potential (ESP) distribution of two conformers of DPE-DDMAc. The positive electrostatic sites mainly localize on the DPE moiety for both molecules which induced moderate electron-withdrawing ability of the DPE unit.

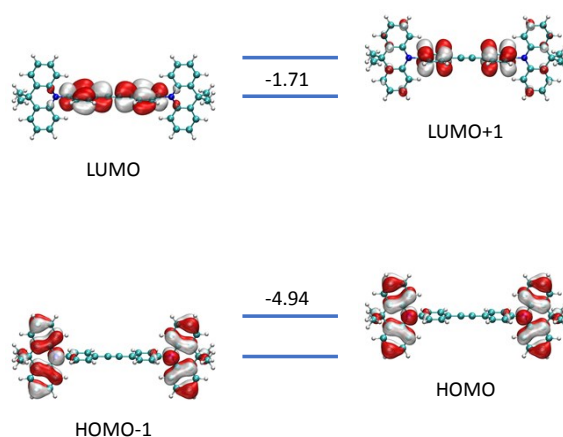


Fig. S12. Frontier molecular orbital distributions of DPE-DDMAc calculated on B3LYP/6-31G* level in gas phase.

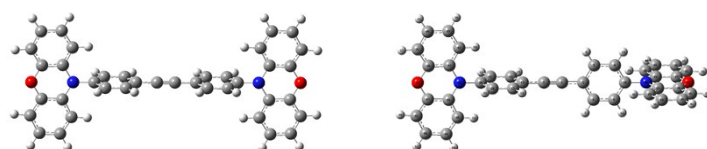


Fig. S13. Front views of horizontal oriented backbone (-1722.38936220 a.u.) and vertical oriented backbone (-1722.38783975 a.u.) DPE-DPXZ optimized in gas phase in B3LYP/6-31G* level. We tentatively took the horizontal oriented backbone one as the initial guess for the subsequent simulation for its ground state energy is lower than the vertical oriented backbone one.

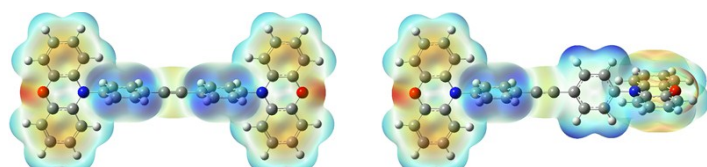


Fig. S14. Electrostatic potential (ESP) distribution of two conformers of DPE-DPXZ. The positive electrostatic sites mainly localize on the DPE moiety for both molecules which induced moderate electron-withdrawing ability of the DPE unit.

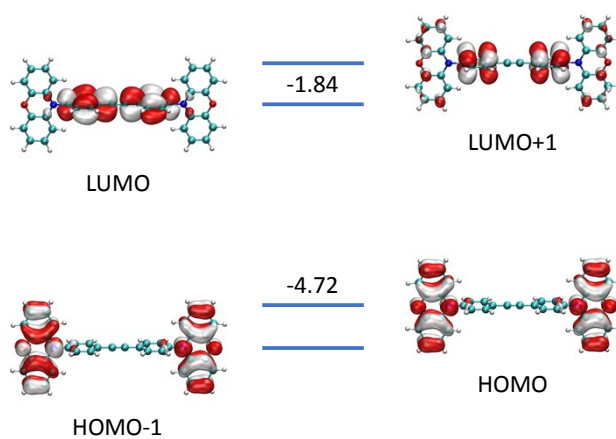


Fig. S15. Frontier molecular orbital distributions of DPE-DPXZ calculated on B3LYP/6-31G* level in gas phase.

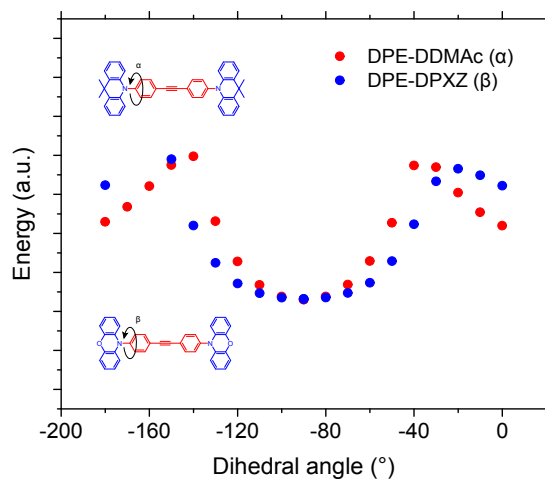


Fig. S16. Potential surface scan of DPE-DDMAc and DPE-DPXZ in gas phase in B3LYP/6-31G* level. The scanning dihedral angles are α for DPE-DDMAc and β for DPE-DPXZ, respectively.



Fig. S17. The molecular conformation of DPE-DDMAc in single crystal structures.

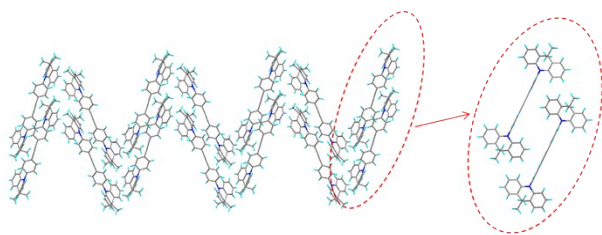


Fig. S18. Molecular packing of DPE-DDMAc in single crystal structures.

Table S1. Photophysical properties of the investigated compounds. a) data measured in toluene solution (0.01 mM); b) data measured in neat film state; c) data measured in doped films (10 wt% in DPEPO); d) calculated results from TD-DFT simulation.

Materials	$\lambda_{\text{abs}}/\text{nm}$	$\epsilon/\text{mM cm}^{-1}$	$\lambda_{\text{PL}}/\text{nm}$	QY/% ^{c)}	$\tau_{\text{F}}/\text{ns}$	$\tau_{\text{TADF}}/\mu\text{s}$	k_{F} ($\times 10^7 \text{ s}^{-1}$)	k_{ISC} ($\times 10^7 \text{ s}^{-1}$)	k_{IC} ($\times 10^7 \text{ s}^{-1}$)	k_{TADF} ($\times 10^3 \text{ s}^{-1}$)	$E_{0-0}(S_1)$ (eV)	$E_{0-0}(T_1)$ (eV)	$\Delta E_{\text{ST}}/\text{eV}$
DPE-DDMAc	355 ^{a)} /363 ^{b)}	3.60 ^{a)}	428 ^{a)} /415 ^{b)} /433 ^{c)}	23.0/25.0 (± 3.0)	6.70 ^{c)}	/	3.73 ^{c)}	11.2 ^{c)}		/	3.16 ^{a)} , ¹ CT	2.61 ^{a)} , ³ LE	0.55 ^{a)} /0.44 ^{d)}
DPE-DPXZ	381 ^{a)} /390 ^{b)}	3.75 ^{a)}	468 ^{a)} /475 ^{b)} /475 ^{c)}	19.0/30.0 (± 3.0)	5.58 ^{c)}	542.7 ^{c)}	1.79 ^{c)}	11.9 ^{c)}	4.18 ^{c)}	0.55 ^{c)}	2.92 ^{a)} , ¹ CT	2.52 ^{a)} , ³ LE	0.40 ^{a)} /0.18 ^{d)}
DMAc			336 ^{a)}								3.69 ^{a)} , ¹ LE	3.12 ^{a)} , ³ LE	0.57 ^{a)}
PXZ			336 ^{a)}								3.69 ^{a)} , ¹ LE	3.13 ^{a)} , ³ LE	0.56 ^{a)}
DPE			323 ^{a)}								3.84 ^{a)} , ³ LE	2.72 ^{a)} , ³ LE	1.12 ^{a)}

Photo-physical Properties.

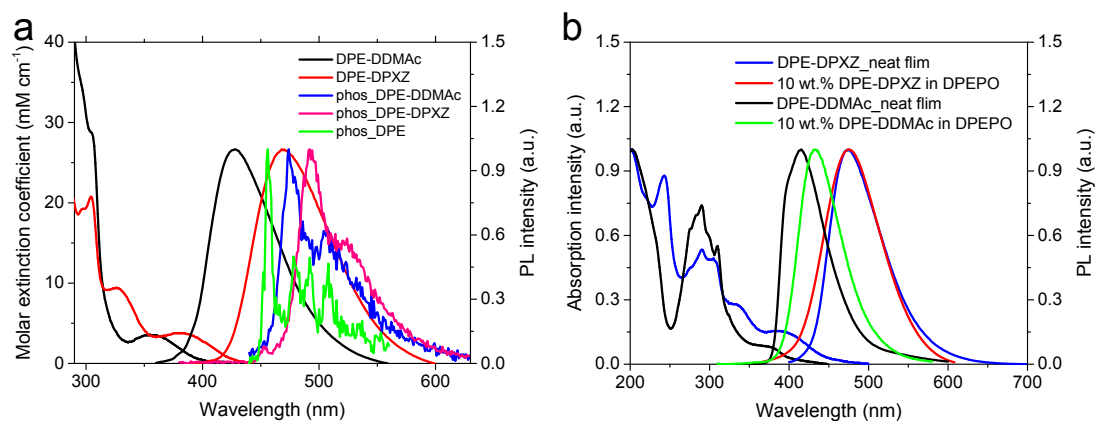


Fig. S19. a, UV-vis, PL and phosphorescence (at 77 K) spectra of the investigated compounds in toluene solution (0.01 mM). b, UV-vis absorption and photoluminescence spectra of neat films and doped films (10 wt% in DPEPO) of compounds DPE-DPXZ and DPE-DDMAc were shown, respectively.

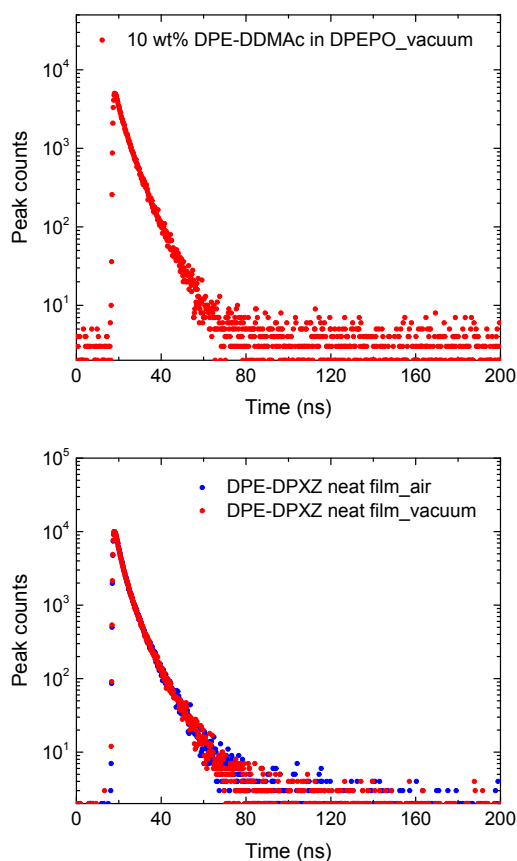


Fig. S20. Transient decay spectra of the investigated compounds measured in air and vacuum condition at room temperature using a fluorescence lifetime spectrometer (C11367-01, Hamamatsu Photonics).

Thermal Properties.

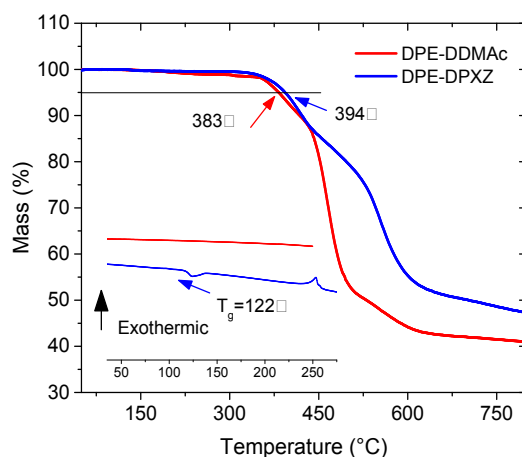


Fig. S21. Thermal properties of DPE-DDMAc and DPE-DPXZ were shown. The corresponding thermal decomposition temperatures (referring to 5% mass loss) were over 380 °C, which were high enough for vacuum evaporation process. For DPE-DPXZ, the glass transition temperature of 122 °C was observed.

Cyclic Voltammetry.

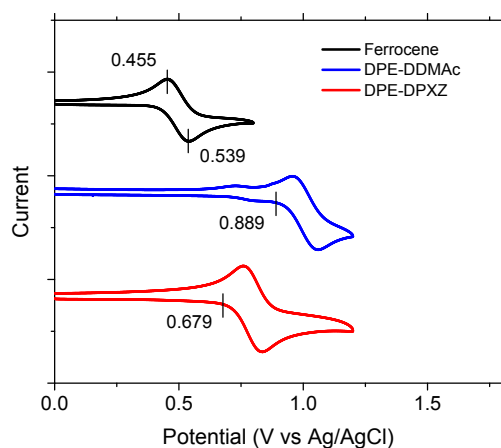


Fig. S22. Cyclic voltammograms of two compounds measured in dichloromethane: acetonitrile (3:1) solution using $n\text{-Bu}_4\text{NPF}_6$ as the supporting electrolyte. The detailed evaluation of ionization potential (IP) and electron affinity (EA) potentials were listed in **Table 1**.

OLED Characterization.

Device Fabrication and Characterization: Glass substrates pre-coated with a 95-nm-thin layer of indium tin oxide (ITO) with a sheet resistance of 10 Ω per square were thoroughly cleaned in ultrasonic bath of acetone, isopropyl alcohol, detergent, deionized water, and isopropyl alcohol and treated with O₂ plasma for 20 min in sequence. Organic layers were deposited onto the ITO coated glass substrates by thermal evaporation under high vacuum ($<5 \times 10^{-4}$ Pa). Cathode, consisting of a 1 nm-thin layer of LiF followed by a 100 nm thin Al layer, was patterned using a shadow mask with an array of 3 mm \times 3 mm openings. Deposition rates are 1–2 \AA s^{-1} for organic materials, 0.1 \AA s^{-1} for LiF, and 6 \AA s^{-1} for Al, respectively. Electroluminescence (EL) spectra were recorded by an optical analyzer, Photo Research PR705. The current density and luminance versus driving voltage characteristics were measured by Keithley 2420 and Konica Minolta chromameter CS-200. EQE was calculated from the luminance, current density, and EL spectrum, assuming a Lambertian distribution.

Table S2. Summary of performances of OLED devices I, II and III.

Device	EBL	V_{ON}^* (V)	Max. Efficiency		EQE_{100}^* (%)	L_{max} (cd m^{-2})	CIE (x, y) (@ 1mA cm^2)
			CE_{max} (cd/A)	EQE_{max} (%)			
I	TAPC	3.8	2.72	2.89	1.14	2599	(0.271, 0.434)
II	TAPC	3.3	7.27	3.52	2.14	5995	(0.176, 0.282)
III	DAcDB	3.4	22.8	10.8	2.58	718	(0.180, 0.314)

* V_{ON} and EQE_{100} are obtained at 1 and 100 cd m^{-2} , respectively.

References

1. M. J. Frisch, G. W. Trucks, H. B. Schlegel, G. E. Scuseria, M. A. Robb, J. R. Cheeseman, G. Scalmani, V. Barone, B. Mennucci, G. A. Petersson, H. Nakatsuji, M. Caricato, X. Li, H. P. Hratchian, A. F. Izmaylov, J. Bloino, G. Zheng, J. L. Sonnenberg, M. Hada, M. Ehara, K. Toyota, R. Fukuda, J. Hasegawa, M. Ishida, T. Nakajima, Y. Honda, O. Kitao, H. Nakai, T. Vreven, J. A. Montgomery Jr, J. E. Peralta, F. Ogliaro, M. J. Bearpark, J. Heyd, E. N. Brothers, K. N. Kudin, V. N. Staroverov, R. Kobayashi, J. Normand, K. Raghavachari, A. P. Rendell, J. C. Burant, S. S. Iyengar, J. Tomasi, M. Cossi, N. Rega, N. J. Millam, M. Klene, J. E. Knox, J. B. Cross, V. Bakken, C. Adamo, J. Jaramillo, R. Gomperts, R. E. Stratmann, O. Yazyev, A. J. Austin, R. Cammi, C. Pomelli, J. W. Ochterski, R. L. Martin, K. Morokuma, V. G. Zakrzewski, G. A. Voth, P. Salvador, J. J. Dannenberg, S. Dapprich, A. D. Daniels, Ö . Farkas, J. B. Foresman, J. V. Ortiz, J. Cioslowski and D. J. Fox, *Gaussian 09, Revision B.01*, 2009, Gaussian, Inc., Wallingford CT, U.S.A.
2. S. Huang, Q. Zhang, Y. Shiota, T. Nakagawa, K. Kuwabara, K. Yoshizawa and C. Adachi, *J. Chem. Theory Comput.*, 2013, **9**, 3872-3877.
3. Q. Zhang, B. Li, S. Huang, H. Nomura, H. Tanaka and C. Adachi, *Nat. Photon.*, 2014, **8**, 326-332.